



Inhalable spray-dried porous microparticles containing dehydroandrographolide succinate phospholipid complex capable of improving and prolonging pulmonary anti-inflammatory efficacy in mice

Wei-Ya Chen^{1,2} · Jia-Xing Wei¹ · Chen-Yang Yu¹ · Chun-Yu Liu¹ · Yong-Hong Liao¹

Accepted: 6 May 2024
© Controlled Release Society 2024

Abstract

Due to the unique physiological barriers within the lungs, there are considerable challenges in developing drug delivery systems enabling prolonged drug exposure to respiratory epithelial cells. Here, we report a PulmoSphere-based dry powder technology that incorporates a drug-phospholipid complex to promote intracellular retention of dehydroandrographolide succinate (DAS) in respiratory epithelial cells following pulmonary delivery. The DAS-phospholipid complex has the ability to self-assemble into nanoparticles. After spray-drying to produce PulmoSphere microparticles loaded with the drug-phospholipid complex, the rehydrated microparticles discharge the phospholipid complex without altering its physicochemical properties. The microparticles containing the DAS-phospholipid complex exhibit remarkable aerodynamic properties with a fine particle fraction of ~60% and a mass median aerodynamic diameter of ~2.3 μm . These properties facilitate deposition in the alveolar region. In vitro cell culture and lung tissue explants experiments reveal that the drug-phospholipid complex prolongs intracellular residence time and lung tissue retention due to the slow intracellular disassociation of drug from the complex. Once deposited in the lungs, the DAS-phospholipid complex loaded microparticles increase and extend drug exposure to the lung tissues and the immune cells compared to the free DAS counterpart. The improved drug exposure to airway epithelial cells, but not immune cells, is related to a prolonged duration of pulmonary anti-inflammation at decreased doses in a mouse model of acute lung injury induced by lipopolysaccharide. Overall, the phospholipid complex loaded microparticles present a promising approach for improved treatment of respiratory diseases, e.g. pneumonia and acute respiratory distress syndrome.

Keywords Phospholipid complex · PulmoSphere microparticles · Acute lung injury · Lung retention · Pulmonary delivery · Sustained release

Introduction

Lower respiratory tract infections are one of the top ten leading causes of death in the world. In particular, the COVID-19 pandemic has resulted in the official global death toll exceeding 6.5 million within three years. The pulmonary pathological features of lower respiratory tract infection diseases, such as acute lung injury and acute respiratory distress syndrome (ARDS), mainly include the injury of pulmonary vascular endothelium and pulmonary epithelium, and the infiltration of pulmonary inflammatory cells [1, 2]. Although systemic administration can deliver drugs to the pulmonary vascular endothelial cells, limited lung penetration generally leads to poor therapeutic outcomes [3]. As a

✉ Yong-Hong Liao
yhliao@implad.ac.cn

¹ Key Laboratory of Bioactive Substances and Resources Utilization of Chinese Herbal Medicines, Ministry of Education, Institute of Medicinal Plant Development, Chinese Academy of Medical Sciences & Peking Union Medical College, 151 Malianwa North Road, Haidian District, 100193 Beijing, China

² Institute of Chinese Materia Medica, China Academy of Chinese Medical Sciences, 100700 Beijing, China

result, there is a vital need to develop or improve delivery systems for enhancing and prolonging the lung exposure of new and existing medications. Pulmonary delivery is known to directly target drugs to the lungs, i.e. pulmonary epithelium and infiltrated inflammatory cells. However, due to the excellent lung epithelial permeability, inhaled small molecules deposited and dissolved in the lung epithelial lining fluid are readily penetrated the epithelium and absorbed into the systemic circulation, limiting the lung retention and local drug exposure [4, 5]. Therefore, increasing and prolonging the exposure of inhaled drugs in the lungs is a key concern for the treatment of lower respiratory tract infections [6–9].

In the literature, various particle carriers, such as polymeric micelles, nanoparticles and microparticles, solid lipid particles/nanostructured lipid carriers and liposomes, have been developed for sustained-release of inhaled drugs [10, 11]. Indeed, earlier studies have demonstrated that such carriers efficiently extended lung exposure and minimized systemic adverse effects, leading to improved local efficacy for lung cancer, respiratory infections, pulmonary hypertension and other respiratory diseases [12–17]. However, there existed significant barriers to clinical translation for the previously documented inhalable carriers. First, except liposomes and phospholipid based particles, the material choices lacked consideration of pulmonary biocompatibility, and hence the particle carriers bear practical limitations as far as the potential pulmonary toxicity is concerned [18–20]. Second, the drug release in the lung seemed far from optimal and often led to poor correlation between pharmacokinetics and pharmacodynamics. Indeed, the *in vivo* lung release of inhaled formulations were largely uninvestigated owing to the inability to differentiate between released drug and drug within a carrier, and hence the total drug content recovered in the lung was generally used to indicate the lung exposure in the literature. Taking inhaled liposomes as examples, pre-clinical studies revealed that liposomal amikacin sustained the lung exposure for 168 h after inhalation, yet the clinical application required a once daily nebulisation therapy [21, 22]. In another work, although inhaled liposomal fasudil extended the therapeutic levels of drug for at least 15 h, pulmonary vasodilation effect only lasted for ~3 h [12]. Third, despite of the record of successful clinical application, liposomes have been shown some limitations regarding stability upon storage and aerosolization, low drug-loading capacity and difficulty in scale-up production [5, 23].

In this study, we report a PulmoSphere-based dry powder technology that incorporates drug-phospholipid complex to promote the cellular uptake and lung retention of dehydroandrographolide succinate (DAS) after pulmonary delivery. DAS is a water-soluble succinate ester derivative of andrographolide and was approved as an injectable

formulation for the treatment of pneumonia together with upper respiratory infections in China due to its immunostimulatory and anti-inflammatory effects [24]. PulmoSphere technology is an emulsion-based spray-drying process that enables to produce highly inhalable porous phospholipid based microparticles and such microparticles have been used in several marketed metered dose or dry powder inhalation products (e.g. Tobin[®] Podhaler[®], a tobramycin inhalation powder; Breztri Aerosphere[®], a budesonide, glycopyrrolate and formoterol fumarate inhalation aerosol) [25–28]. A drug in PulmoSphere particles can exist as molecular dispersion or suspension within a phospholipid matrix. However, the phospholipid coating generally fails to act as a barrier to sustain the drug release, with the release profiles primarily controlled by the inherent dissolution/release characteristics of the loaded drug particles. To improve the lung retention of inhaled DAS, the present study intended to incorporate DAS-phospholipid complex into PulmoSphere particles. Initially, drug-phospholipid complexes were documented as drug delivery system of naturally occurring compounds, which interact with phospholipid molecules to form phyto-phospholipid complexes, commonly known as phytosomes. The formation of these complexes has been attributed to the establishment of chemical bonds, such as ionic or hydrogen bond and/or hydrophobic interactions, between the phytochemicals and phospholipid molecules [29–31]. The objectives of this study were to investigate whether spray-dried PulmoSphere-based microparticles containing phospholipid complex could offer both superior inhalability and prolonged lung exposure, leading to enhanced anti-inflammatory potency and an extended duration of action.

Materials and methods

Materials

Potassium dehydroandrographolide succinate (DAS, HPLC ≥ 98%) was purchased from Shanghai Yuanye Bio-Technology Co., Ltd. (Shanghai, China). 1,2-Dioctadecanoyl-sn-glycero-3-phosphocholine (DSPC), 1-Bromoheptadecafluorooctane (PFOB) and Rhodamine B (RB) was bought from Shanghai Macklin Biochemical Co., Ltd (Shanghai, China). Fluorescein isothiocyanate modified 1, 2-distearoyl-sn-glycero-3-phosphoethanolamine (FITC-DSPE) was obtained from Xi'an Ruixi Biological Technology Co., Ltd (Xi'an, China). Soy phosphatidylcholine (SPC) was received from Shanghai Advanced Vehicle Technology Pharmaceutical Ltd. (Shanghai, China). Modified Eagle's Medium (MEM), fetal bovine serum (FBS), phosphate buffer saline (PBS), penicillin-streptomycin solution (P/S) and non-essential amino acids (NEAA) were purchased from

Gibco. Krebs-Ringer buffer, 4',6-diamidino-2-phenylindole (DAPI) and lipopolysaccharide (*Escherichia coli* O55:B5, LPS) were bought from Beijing Solarbio Science & Technology Co., Ltd. (Beijing, China). Mouse tumour necrosis factor- α (TNF- α) and mouse interleukin-6 (IL-6) ELISA kits were obtained from Neobioscience Technology Co., Ltd (Beijing, China). Formic acid was obtained from Dikma Co., Ltd. (Beijing, China). Acetonitrile and methanol of HPLC grade were purchased from Thermo Fisher Scientific Inc. (Waltham, MA, U.S.A.). All other chemicals and reagents were of analytical grade.

Synthesis of phospholipid complex

DAS and DSPC were reacted under a molar ratio of 1:1 and 1:2 in a mixed solvent of methanol: chloroform (1:4) at 2.5 mg/ml DAS under stirring at 40 °C for 2 h. Then the organic solvent was removed completely after rotary evaporation and vacuum drying overnight to obtain dried DAS phospholipid complex (DAS-PC), which was then dispersed in water to form nano-sized DAS-PC suspension under sonication at 65 °C for 5 min.

RB and SPC were reacted in tetrahydrofuran under stirring at 50 °C for 2 h and then subjected to evaporation under vacuum. The residue was re-dissolved in the petroleum ether and filtered to remove the unreacted RB. After the thorough removal of the organic solvent, the RB-SPC complex (RB-PC) was dispersed in water and self-assembled into nanoparticles under sonication. For the preparation of fluorescein isothiocyanate (FITC) labelled RB-PC, FITC-DSPE was incorporated into RB-PC to form nanostructures together.

Characterization of phospholipid complex

The particle size and zeta potential of DAS-PC and RB-PC were measured by dynamic light scattering (DLS) and a Zetasizer Nano ZS system (Malvern Instruments Ltd., UK). The morphology of nanoparticles was observed on a JEM 1200EX transmission electron microscope (TEM) after negative staining with 2% uranyl acetate solution. Differential scanning calorimetry (DSC), Fourier transform infrared (FTIR) and ultraviolet-visible (UV) spectroscopy were used to analyse the changes in thermodynamic and spectroscopy

properties caused by the formation of complex. The DSC analysis (DSC, Q200, TA Instruments, USA) was carried out with the temperature heating from 40 to 250 °C at a constant rate of 10 °C/min. The infrared spectra were determined by FTIR spectroscopy (FTIR-8400 S, Shimadzu, Japan) with a scanning range from 4000 to 400 cm^{-1} by using of the KBr method. The UV spectrophotometer (Cary 100, Agilent, USA) was used to obtain the UV spectra (in methanol) in the range from 200 to 300 nm. ^1H NMR (Avance III 600 MHz spectrometer, Bruker, America) spectra were also obtained to explore the action sites between drugs and phospholipids deuteriochloroform (CDCl_3) as well as the self-assembly mechanism in deuterated water.

Preparation of spray-dried porous microparticles

The spray-dried blank phospholipid particles (SDPP) and DAS particles (DAS@SDPP) were prepared by a two-step process described previously [25]. Briefly, an aliquot of 150 mg DSPC was dispersed in 9 ml hot water (65 ~ 70 °C) containing 10.5 mg CaCl_2 under shearing with a hand-held homogenizer (F6/F10, Shanghai Jingxin, China) at 8000 rpm for ~ 5 min. An aliquot of 3.75 g PFOB was then added dropwise under mixing for 5 min to form a coarse emulsion which was then homogenized under high pressure (18,000 psi) for five cycles using a homogenizer (JN-Mini Pro, JNBIO, China). The resulting fluorocarbon-in-water emulsion had a mean hydrodynamic particle size of ~ 184 nm. The PFOB emulsion was then mixed with 20 ml water or 5 mg/ml DAS aqueous solution and the mixtures were spray-dried with a standard B-290 Mini spray-drier (Buchi, Flawil, Switzerland) under the following conditions: inlet temperature 110 °C; aspirator 100%; feed rate 2.5 ml/min; nitrogen flow 1744 L/h.

For the preparation of spray-dried DAS-PC loaded particles (DAS-PC@SDPP), an aliquot of 50 mg DSPC/3.5 mg CaCl_2 /1.25 g PFOB was used to prepare the PFOB emulsion whereas the DAS-PC suspension was obtained by the reaction between 100 mg DAS and 100 mg DSPC following the protocols described in Sect. 2.2. Upon mixing the 5 mg/ml DAS-PC suspension (calculated by DAS) with PFOB emulsion, the mixture was spray-dried following the above condition. The compositions of various formulations investigated were summarized below (Table 1).

Characterization of spray-dried porous microparticles

Scanning electron microscopy (SEM, JSM-6510LV, JEOL, Japan) was used to observe the particle morphology at 15 kV after gold sputter-coating. The thermodynamic and spectroscopy properties of the preparations were analysed

Table 1 The compositions of various formulations

Formulations (% wt/wt)	DAS (%)	DSPC (%)	CaCl_2 (%)
DAS	100	0	0
DAS-PC	33.3	66.7	0
SDPP	0	93.0	7.0
DAS+SDPP	38.4	57.6	4.0
DAS@SDPP	38.4	57.6	4.0
DAS-PC@SDPP	39.4	59.2	1.4

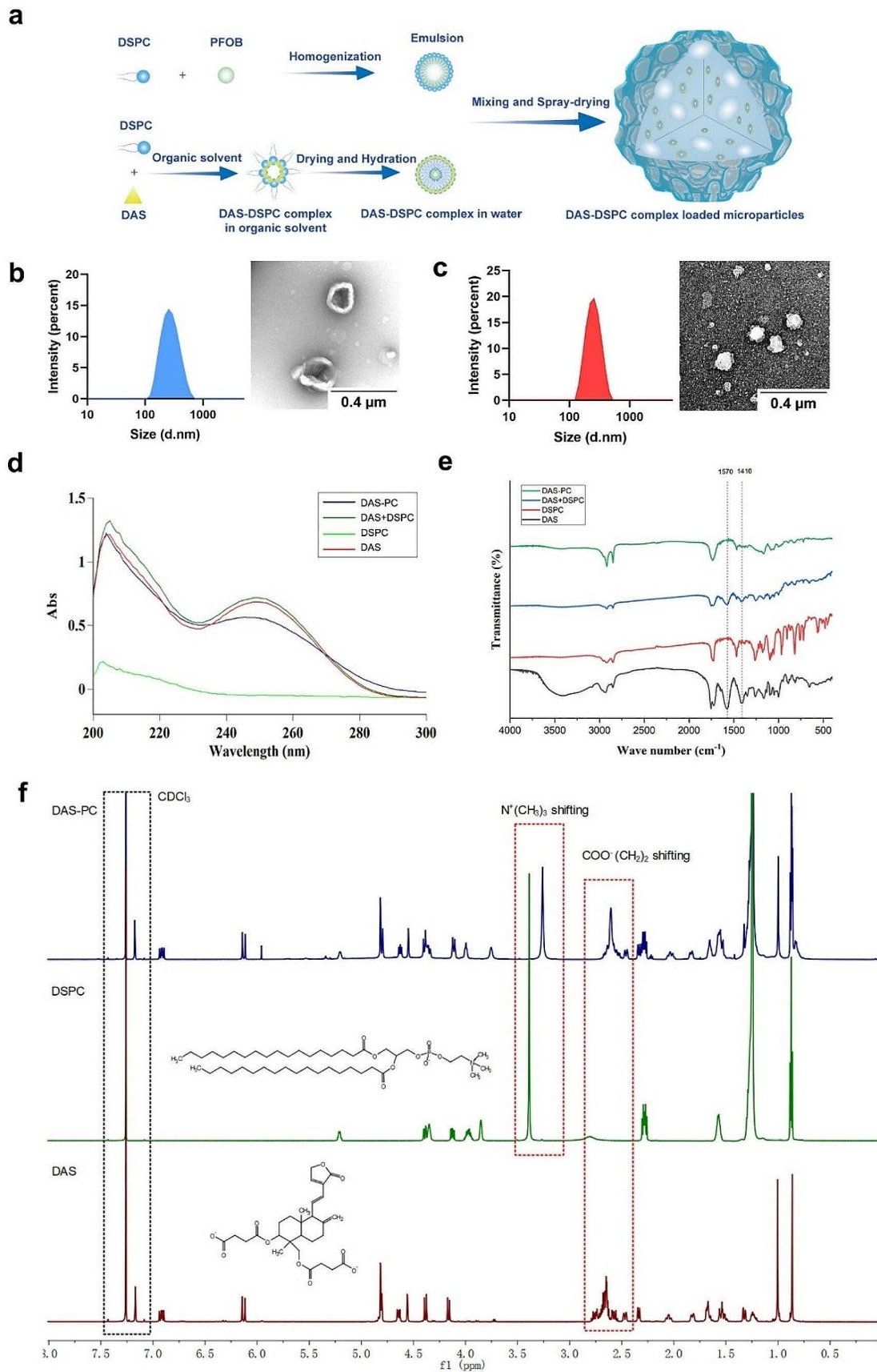


Fig. 1 Characterization of Phospholipid Complex. (a) Schematic diagram of preparation process, including synthesis and hydration of phospholipid complex, and preparation of DAS-PC@SDPP. Particle size and morphology of DAS-PC (b) and RB-PC (c). Ultraviolet spectra (d) and infrared spectra (e) of DAS, DSPC, their physical mixture and DAS-PC. (f) ^1H NMR spectra of DAS, DSPC and DAS-PC

by DSC and FTIR. The drug loading was determined using an HPLC method (SI, S2) after spray-dried powders was weighed and dissolved in methanol. DAS-PC@SDPP was redispersed in water and filtered by 0.45 μm membrane to recover DAS-PC nanoparticles. The particle size, zeta potential and morphology of the recovered nanoparticles were analysed by the Zetasizer Nano ZS system and TEM.

Determination of encapsulation efficiency and relative solubility

The encapsulation efficiency, defined as the analysed proportion of drug content encapsulated in the phospholipid complex, was determined using a centrifugal ultrafiltration method. Briefly, to simulate the conditions within the lung epithelial lining fluid (ELF), ~ 2 mg powders of physical mixture of DAS and SDPP, DAS@SDPP and DAS-PC@SDPP in the same drug-phospholipid ratio were uniformly dispersed in 0.2 ml water and allowed to equilibrium for 15 min. DAS solution and DAS-PC suspension with equivalent DAS concentration to the powders served as controls. The dispersion was transferred into an ultrafiltration tube (100 k Da, Millipore) and centrifuged at 5000 rpm for 5 min, followed by adding 0.4 ml water to the ultrafiltration tube and centrifuging for 10 min. The residual solid in the ultrafiltration tube was recovered by adding methanol and water and the drug was extracted by sonication for 3 min and centrifuge at 12,000 rpm for 5 min. Drug content in the lower filtrate (C_L) and the upper residual solid (C_U) was determined by the HPLC method and the encapsulation efficiency was calculated by

$$\text{Encapsulation Efficiency} = \frac{C_U}{C_U + C_L} * 100\%$$

Following the preparation of powder dispersions, an aliquot of 0.6 ml dichloromethane was added to the dispersion, DAS solution and DAS-PC suspension to extract DAS. Drug content in dichloromethane layer (C_1) and water layer (C_2) were determined by the HPLC method and the relative solubility in dichloromethane was calculated as:

$$\text{Relative Solubility} = \frac{C_1}{C_1 + C_2} * 100\%$$

Evaluation of in vitro aerodynamic properties

The aerodynamic properties of DAS@SDPP and DAS-PC@SDPP were determined using a Next Generation Pharmaceutical Impactor (NGI, COPLEY Scientific, UK). Briefly, approximately 2 mg microparticles were weighed and loaded into size 3 capsules which were placed in a Handihaler[®]. The inhaler was attached to the NGI via a rubber mouthpiece. Subsequently, the device was activated to disperse particles into NGI at a flow rate of 60 L/min for 4 s intervals. Prior to each assessment, a thin layer of glycerol was coated onto the stages of NGI to reduce particle bounce. After 4 s suction of one capsule, the NGI was dismantled and the particles deposited on inhaler, capsule, mouthpiece, throat, and each stage of NGI were collected and dissolved by water. The recovered dose was defined as the total amount of drug recovered from all components (including capsules, artificial throats, and each stage of the NGI) during a single run of the impaction process. The percentage of emitted dose was the fraction of drug that exited the inhaler (i.e. in mouthpiece, throat and the impinger) as a percentage of the recovered dose. The fine particle fraction (FPF) referred to the percentage of the drug mass with aerodynamic diameter of particles < 5 μm compared to the total emitted dose. The Mass median aerodynamic diameter (MMAD) was a 50% cumulative percentage of aerodynamic diameters and the GSD was geometric standard deviation calculated by CIT-DAS (UK Copley Inhaler Data Analysis Software).

In vitro drug release of spray-dried particles

The dissolution/release profile of DAS@SDPP and DAS-PC@SDPP was investigated using a Franz diffusion cell [32]. This cell was separated into a donor chamber and a receiver chamber by a glass fibre filter membrane (GF/C grade, Whatman). In the donor chamber, 0.2 ml of release medium was introduced to mimic the minimal aqueous environment of the lung epithelial lining fluid, whereas the receiver chamber (contained ~ 10.5 ml of water) functioned solely as a reservoir, collecting the drug that dissolved/released in the donor chamber and subsequently diffused through the membrane. Bulk DAS powder and the physical mixture of DAS and SDPP were set as control groups. To initiate the release process, the drug preparations were evenly dispersed on a pre-hydrated filter membrane within the donor chamber. The temperature was maintained at 37 $^{\circ}\text{C}$ and the receiver medium was stirred at 100 rpm with a magnetic bar. At pre-determined time intervals (5, 15, 30, 60, 120, 240, 480 and 720 min), 0.5 ml of dissolution medium was withdrawn and an equal volume of pre-warmed fresh medium was refilled immediately. The concentration of DAS was quantified by HPLC.

In vitro lung affinity test

The in vitro lung affinity test was performed following a previous protocol [33]. Fresh rat lung tissues were cut into small pieces (about 1 mm³). An aliquot of ~100 mg lung explants and 0.9 ml Krebs-Ringer buffer was added to each well of a 24-well plate. DAS solution or DAS-PC suspension (200 µg/ml DAS, 0.1 ml) was added to each plate and shaken for 2 min at 300 rpm before incubation at 37 °C. The buffer and lung explants in each plate were collected after 10, 25, 40–60 min incubation, respectively. The lung explants were washed by saline to rinse off the drug adhered to the surface and then homogenized in methanol to extract the drug inside. All the samples were centrifuged at 12,000 rpm for 5 min before being taken for HPLC analysis.

The desorption properties were investigated by firstly incubating the lung explants with DAS solution or DAS-PC suspension (200 µg/ml DAS) for 60 min following the protocols of adsorption experiment above. Then the lung explants were washed and transferred to 1 ml blank buffer. After 15, 30, 60–120 min incubation at 37 °C, the buffer and lung tissue in each plate were collected respectively and the drug concentrations in the buffer (C_{buffer}) and lung tissue ($C_{\text{lung tissue}}$) were detected. The pulmonary permeability parameter K_p of the drug was calculated as $C_{\text{lung tissue}} (\mu\text{g/g lung tissue}) / C_{\text{buffer}} (\mu\text{g/ml})$ and the drug dissociation rate constant (K_d) as $0.693/T_{1/2}$. The desorption curves of K_p versus time were obtained and the dissociation half-life $T_{1/2}$ was determined by a DAS 2.0 software (Mathematical Pharmacology Professional Committee of China, Shanghai, China).

In vitro release and disassociation of phospholipid complex

FITC labelled RB-PC and the physical mixture of RB and FITC labelled phospholipid were added to dialysis bag (3500 Da cut-off MW) and stirred in release medium (200 ml water) at 37 °C. At pre-determined time intervals (5, 15, 30, 60, 120, 240 and 480 min), 30 µL of dispersion inside the dialysis bag was withdrawn to detect the fluorescence intensity of RB and the fluorescence resonance energy transfer (FRET) signal with fluorescence spectrometer (FL970, Techcomp, China). For determining the latter, the diluted dispersion was excited at 490 nm, the emission spectrum from 505 nm to 650 nm was recorded with two emission peaks (one at 520 nm for FITC, and the other at 570 nm for RB) being detected. FRET was expressed as the emission fluorescence intensity (FI) ratio of $FI_{570}/(FI_{520} + FI_{570})$ [34].

Cellular uptake and release of phospholipid complex

The Calu-3 cells were cultured in an incubator at 37 °C, 5% CO₂ with Modified Eagle's Medium (MEM) supplemented with 10% fetal bovine serum (FBS), 1% non-essential amino acids (NEAA) and 1% penicillin-streptomycin solution. The Calu-3 cells were uniformly seeded in each well at a density of 5×10^4 and incubated for 24 h in a 24-well plate, and then the medium was replaced with MEM containing FITC labelled RB-PC and the physical mixture of RB and FITC labelled phospholipid at RB concentration of 2 µg/ml (SI, Cell Viability Assay). The supernatant was removed at 0.5, 1 and 2 h post incubation, and the cells were washed 3 times with PBS, fixed in 4% paraformaldehyde for 10 min, and stained with 4',6-diamidino-2-phenyl-indole (DAPI) for further observation. In addition, after the cells were subjected to cellular uptake for 2 h and followed by washing with buffer, the cells were replaced with blank medium to incubate for further 0.5, 1, 2 and 4 h for the determination of cellular release. At each time point, the cells were also fixed in 4% paraformaldehyde and stained with DAPI. Subsequently, the fixed cells were observed using a confocal microscope (TCS SP8, Leica, Germany). DAPI, FITC and RB were detected by 405 nm, 488 nm and 547 nm excited optical channels, respectively. When shooting FRET, the donor was set to the excitation wavelength of FITC and the acceptor was set to the emission wavelength of RB within the FRET AB system. The semi-quantitative analysis of fluorescence intensity was carried on with ImageJ developed by Wayne Rasband (<http://imagej.nih.gov/ij>).

Animals

Male BALB/c mice (18–22 g) were provided by Beijing Vital River Laboratory Animal Technology Co. Ltd (Beijing, China). All animals were allowed to acclimatize to laboratory conditions for at least 7 days with free access to food and water in a specific pathogen-free animal room. Animal procurement and experiments were subjected to approval by the Animal Ethics Committee of the Institute of Medicinal Plant Development, Chinese Academy of Medical Sciences & Peking Union Medical College, ethical approval number SLXD-20,211,025,012.

Intratracheal administration to mice

The procedure of intratracheal administration of dry powder to mice was referred to the literature [35, 36] with modification. Briefly, all mice were anesthetized with intraperitoneal injection of sodium pentobarbital (40 mg/kg) and fixed on an endotracheal intubation platform. A 22 G cannula tube

with a plastic guiding cannula outside was inserted into the trachea under visual guidance. The guiding cannula could act as a protective shield to prevent any secretion or moisture in the trachea from contaminating or blocking the 22 G cannula tube tip to insufflate dry powders. Different dry powder preparations (~2 mg) were weighed to achieve doses of 2.2 mg/kg, 6.6 mg/kg or 20 mg/kg DAS and loaded into the cannula tube before inserting. Before the delivery of 2.2 mg/kg or 6.7 mg/kg doses of DAS, the powders were diluted with blank phospholipid particles. Plastic syringe was filled with 0.3 ml air and dry powder loaded was blown into the lung of mice thoroughly. As for the liquid preparation, 50 μ l of fluid was added to the cannula tube after inserting in the tracheal of mice and inhaled by mice [37].

Pulmonary retention of phospholipid complex

Mice were intratracheally dosed with RB solution physically mixed with soy phosphatidylcholine or RB-PC dispersion (at a dose of 2 mg/kg RB) and sacrificed at 0.5, 1, 3, 6 and 12 h after administration. Lung tissue was harvested and subjected to *ex vivo* imaging with an excitation wavelength at 550 nm and emission wavelength at 570 nm under an *in vivo* imaging system (IVIS, Caliper Life Sciences, USA).

Lung distribution of DAS formulations

Mice were randomly divided into four groups including DAS solution, the physical mixture of DAS and SDPP, DAS@SDPP and DAS-PC@SDPP and administrated at the dose of 20 mg/kg DAS *via* intratracheal route. At predetermined time points (0.25, 1, 3, 6 and 12 h) post-dosing ($n=4$), 0.5 ml blood was collected and the plasma was obtained immediately after 10 min centrifugation at 5000 rpm. Subsequently, the mice were sacrificed by euthanasia and the bronchoalveolar lavage fluid (BALF) was collected by inserting a flat tip needle into the tracheal with 0.8 ml saline and repeated 3 times. The BALF was centrifuged at 5000 rpm for 10 min to separate the BALF supernatant and the cell pellet. Afterward, lung tissue was removed and weighed.

The extraction of DAS from plasma and lung tissue samples was performed following our previous protocols [24]. The BALF was diluted 5-fold by acetonitrile and the supernatants after centrifugation were analysed by LC-MS/MS (SI, S3). The ELF referred to the epithelial lining fluid of the lungs, whereas the BALF represented the bronchoalveolar lavage fluid, which was the diluted ELF after lavage. In order to determine the drug concentration in the ELF, the concentrations of urea in plasma and BALF were analysed according to the urease-glutamate dehydrogenase method with a commercially available kit (BIOSINO, China) on AU480 automatic biochemical analyser (Beckman Coulter,

Inc., USA). Assuming the urea concentrations in the ELF and plasma were equal, the drug concentration in the ELF was calculated as $C_{\text{BALF}}^* (\text{urea}_{\text{plasma}} / \text{urea}_{\text{BALF}})$.

For the determination of drug concentration in cells, the cell pellet from the BALF was subjected to red blood cell lysis and the rest cells were counted (~85% alveolar macrophages). The cell volume was calculated based on an index of $2.42 \mu\text{l}/10^6$ cells [38]. The cells were subsequently broken by an ultrasonic crusher in methanol and the supernatants were subjected to LC-MS/MS analysis.

Pulmonary anti-inflammatory efficacy study

To determine time-dependent anti-inflammatory efficacy, mice were randomly divided into 5 groups: control group, model group, DAS solution, DAS@SDPP and DAS-PC@SDPP group. The mice received DAS solution, DAS@SDPP or DAS-PC@SDPP *via* intratracheal delivery at the dose of 20 mg/kg DAS, respectively. At 1, 3, 6–12 h post-dosing ($n=3$), the pulmonary inflammation was induced by intratracheally dosing LPS at a dose of 500 $\mu\text{g}/\text{kg}$ [39]. Mice were administered with normal saline (NS) or blank SDPP as control.

For determining dose-dependent anti-inflammatory efficacy, mice were administrated with DAS@SDPP and DAS-PC@SDPP *via* pulmonary route at different doses of 2.2, 6.7, 20 mg/kg at 12 h before LPS challenge ($n=3$).

At 6 h after LPS challenge, the mice were sacrificed and the BALF and lung tissue were collected. The BALF samples were centrifuged (12,000 rpm, 5 min) to obtain supernatants and the level of TNF- α and IL-6 in BALF was determined by a mouse TNF- α or IL-6 ELISA kit. The lung tissue was fixed in 4% paraformaldehyde at room temperature for more than 24 h before it was embedded with paraffin wax and sectioned into 5–10 μm slices. Then the lung tissue sections were observed under microscope after hematoxylin and eosin (H&E) staining.

Data analysis

Data were expressed as mean \pm standard deviation (SD) from at least three replicates. Pharmacokinetic parameters such as C_{max} , T_{max} , $T_{1/2}$ (terminal elimination half-life), $\text{AUC}_{0-\infty}$, MRT (mean residence time) were calculated with a DAS 2.0 software by analysing the concentration-time profile with a non-compartmental model. The Origin software was used to fit and calculate the data from ELISA test. A significant difference between data from different groups was statistically processed by one-way analysis of variance (ANOVA) with prism 8.0 and a p -value < 0.05 was regarded as statistically significant.

Results

Preparation and characterization of phospholipid complex

In this work, a semi-synthetic drug, dehydroandrographolide succinate (DAS), and a synthetic dye, rhodamine B (RB), were found to form phospholipid complexes, i.e. DAS and RB phospholipid complexes (DAS-PC and RB-PC), respectively, after reaction with phospholipid. In addition, the complexes appeared to self-assemble into nano-sized particles after rehydration as illustrated in Fig. 1a. The hydrodynamic particle size of DAS-PC and RB-PC were ~ 288 nm and ~ 244 nm, respectively and the TEM images also confirmed the presence of nanostructure for both phospholipid complexes (Fig. 1b and c).

The formation of DAS-PC was confirmed by different spectroscopy and differential scanning calorimetry (DSC). In ultraviolet (UV) spectra, the formation of phospholipid complexes generally resulted in hypochromic effects due to the steric hindrance caused by the interactions between phospholipids and drugs [40]. As shown in Fig. 1d, both DAS and the physical mixture of DAS and DSPC exhibited an absorption peak at 251 nm and yet this peak diminished markedly in the spectrum of DAS-PC. In the infrared spectra (Fig. 1e), DAS showed characteristic bands for the carboxylate groups (COO^-) at 1570 cm^{-1} and 1410 cm^{-1} , attributable to asymmetrical and symmetrical vibrations of the carboxylate, respectively [41]. The typical bands were observed in the physical mixture but disappeared in the DAS-PC, indicating that the carboxylate groups of the drug interacted with phospholipids. Indeed, it has been previously demonstrated that when a carboxylate group interacts with an N^+ group, the absorption band at $1500\text{--}1600\text{ cm}^{-1}$ shifts to $1680\text{--}1750\text{ cm}^{-1}$ [42]. The interactions between carboxylate and N^+ groups were also indicated by ^1H NMR spectra (Fig. 1f). In the ^1H NMR spectra of DAS-PC, the proton signals attributed to the methylene groups attached to carboxylate in DAS shifted from $\delta 2.65$ ppm to $\delta 2.60$ ppm with apparent variations in coupling constant whereas the proton signals of $-\text{N}(\text{CH}_3)_3^+$ in phospholipids at $\delta 3.39$ ppm were broadened and upfield shifted to $\delta 3.26$ ppm. Such findings indicated that the carboxylate groups were involved in the formation of DAS-PC by forming intermolecular ionic interactions [43, 44]. In the mass spectrometry (SI, Fig. S1), DAS-PC exhibited an ion peak at m/z 1322 ($M_{\text{DAS-DSPC}} + \text{H}$) $^+$. In the DSC thermograms (SI, Fig. S2), DSPC had an endothermic peak at $128\text{ }^\circ\text{C}$, whereas DAS had a sharp characteristic endothermic peak (melting point) at $160\text{ }^\circ\text{C}$. After the formation of DAS-PC, these endothermic peaks decreased to $70\text{ }^\circ\text{C}$, indicating the interaction between drug and phospholipid.

Moreover, by comparing the ^1H NMR spectrum of the complex in D_2O with that in deuterated chloroform (SI, Fig. S3), the proton signals attributable to the hydrophobic fat chains of phospholipid and hydrophobic groups of DAS weakened or disappeared whereas the proton signals of the hydrophilic groups at $\delta 3\text{--}4.5$ ppm could be clearly observed. Such findings suggested that DAS-PC produced self-assembled nanostructures with hydrophobic core upon rehydration.

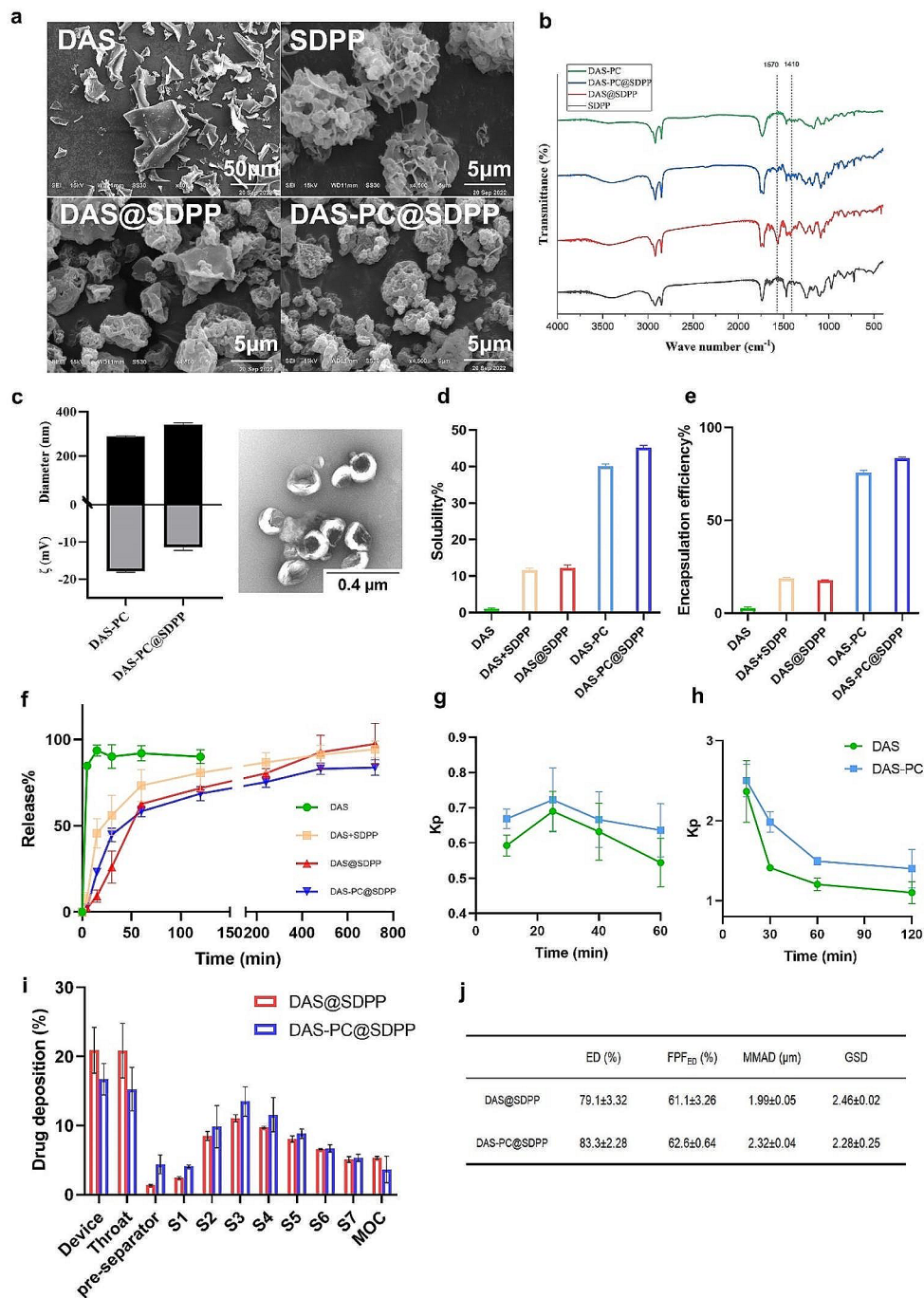
The formation of RB-PC was also confirmed by UV (SI, Fig. S4), and NMR (SI, Fig. S5 and S6) spectroscopy. These spectroscopic data revealed that the mechanism underlying the formation of phospholipid complexes involved intermolecular ionic interactions between the carboxylate groups of RB and the $-\text{N}(\text{CH}_3)_3^+$ moieties of phospholipids. Despite structural differences in their hydrophobic tails, SPC and DSPC shared an identical hydrophilic head, making it unlikely that these differences significantly impact drug-phospholipid interactions. Consequently, RB-SPC was deemed a suitable fluorescent surrogate for elucidating the release mechanism of DAS-DSPC.

Preparation and characterization of spray-dried microparticles

In this work, spray-dried blank particles (SDPP) and DAS particles (DAS@SDPP) were prepared by spray-drying of emulsions with or without the addition of DAS whereas spray-dried DAS-PC loaded particles (DAS-PC@SDPP) is illustrated in Fig. 1a. The drug loading of DAS@SDPP and DAS-PC@SDPP were determined to be $\sim 40\%$, which was also equivalent to the composition ratio in the feed. SEM images showed that the spray-dried particles were porous with corrugated surfaces and the geometric particles size was largely in the range of $3\text{--}10\text{ }\mu\text{m}$ (Fig. 2a).

Subsequently, the effects of spray-drying process on the physicochemical properties of DAS-PC were evaluated. In the infrared spectra (Fig. 2b), the characteristic bands of carboxylate existed in DAS@SDPP, suggesting the lack of formation of complex. In contrast, both DAS-PC and DAS-PC@SDPP showed the disappearance of the characteristic bands, indicating that DAS-PC remained intact after spray-drying. After rehydration of DAS-PC@SDPP, the morphology, particle size and zeta potential of recovered nano-sized DAS-PC were similar to those of DAS-PC before spray-drying (Fig. 2c). The formation of drug-phospholipid complex could change the solubility of hydrophilic drugs in non-polar solvents and encapsulate the drug in the complex. In this work, DAS was poorly soluble in dichloromethane with a relative solubility less than 1.0% of nominal amount of DAS, whereas the solubility of DAS in DAS-PC (DAS: PC 1:1) was more than 40%. After spray-drying,

Fig. 2 Characterization of Spray-dried microparticles. **(a)** Physical morphology of DAS, SDPP, DAS@SDPP and DAS-PC@SDPP under scanning electron microscopy. **(b)** Infrared spectra of SDPP, DAS@SDPP and DAS-PC@SDPP. **(c)** The particle size and zeta potential of DAS-PC before and after spray drying and rehydration as well as its morphology after the rehydration of DAS-PC@SDPP. **(d)** Relative solubility in dichloromethane and **(e)** encapsulation efficiency of DAS, physical mixture of DAS and SDPP, DAS@SDPP, DAS-PC@SDPP and DAS-PC. **(f)** In vitro release of DAS, physical mixture of DAS and SDPP, DAS@SDPP and DAS-PC@SDPP in aqueous solutions. Adsorption kinetic **(g)** and desorption kinetic **(h)** of DAS and DAS-PC with lung tissue *ex vivo*. The aerosol performance **(i)** and aerodynamic parameters **(j)** of DAS@SDPP and DAS-PC@SDPP evaluated by Next Generation Impactor at 60 L min⁻¹



the solubility of DAS in DAS-PC@SDPP was slightly different from that in DAS-PC. The presence of phospholipid increased the solubility of DAS and the solubility of DAS in DAS@SDPP or in the physical mixture of DAS and SDPP were similar (~12%) (Fig. 2d). The encapsulation efficiency was evaluated by centrifugal ultrafiltration. The results (Fig. 2e) showed that the presence of phospholipid tended to encapsulate DAS up to 18%. Upon the formation of DAS-PC, the encapsulation efficiency increased to more

than 75% and the spray-drying process slightly increased the encapsulation efficiency to 83%. Taken together, these findings suggested that DAS-PC was generally stable during spray-drying.

In vitro release data (Fig. 2f) showed the liberation of DAS or DAS-PC from the porous microsphere carrier after rehydration. DAS-PC, due to its nanoscale dimensions, was able to traverse the filter membrane efficiently. The bulk DAS powders dissolved rapidly, achieving a release of 85%

within 5 min, attributed to its exceptional water solubility. However, the introduction of phospholipids resulted in a delayed drug release profile. The physical mixture of DAS and SDPP exhibited a rapid initial release of $\sim 73\%$ within the first hour, whereas DAS@SDPP and DAS-PC@SDPP showed a release of around 60% during the same period. Subsequently, all phospholipid-based formulations exhibited a sustained release pattern, extending up to 12 h. The delayed drug release observed in the physical mixture and DAS@SDPP might be attributed to intermolecular ionic interactions between DAS and DSPC.

The lung tissue explant model was used to evaluate the tissue-to-buffer partition coefficient (K_p) and dissociation rate coefficient (K_d), two metrics indicative of lung tissue affinity of drug [45]. In the adsorption kinetic tests, the K_p ($C_{\text{Lung}}/C_{\text{Buffer}}$) was used as an indicator to reflect the drug distribution to lung tissues with a higher K_p value indicating a higher amount of drug adsorption and a better affinity with the lung tissues [46]. In this work, DAS rapidly penetrated into the lung tissues and reached a plateau within 10 min (Fig. 2g). There were no significant differences in K_p values from 10 min to 60 min. Although DAS-PC always conferred slightly higher K_p values than DAS solution, there were no significant differences in K_p values between DAS solution and DAS-PC. In the desorption kinetic test, the binding drug from DAS solution seemed to disassociate from the lung tissues more rapidly than that from DAS-PC (Fig. 2h). As far as the dissociation rate was concerned, the K_d value of 0.49 conferred by DAS-PC was only \sim half of the K_d (0.97) by DAS solution. The decreased K_d value indicated that DAS-PC improved lung affinity and prolonged lung retention.

After DAS@SDPP and DAS-PC@SDPP were incorporated into carrier-free DPI formulations, *in vitro* studies were conducted to evaluate the aerosol performance of the DPI formulations and results are shown in Fig. 2i and j. The *in vitro* deposition profiles of DPI formulations prepared from either DAS@SDPP or DAS-PC@SDPP were similar, demonstrating a similar aerodynamic behaviour for the two spray-dried particles (Fig. 2i). In addition, both DPI formulations exhibited excellent FPF (58–60%) and had optimal MMAD values (1.99–2.32 μm) (Fig. 2j). FPF and MMAD are regarded as useful parameters to predict the lung deposition profiles of inhaled aerosols. FPF dictates the total lung deposition with deposition increasing as FPF increases, whereas MMAD influences regional deposition. Microparticles with MMAD in the range of 1–3 μm are suitable for delivery to the lung periphery [47, 48].

Fig. 3 Release kinetics of phospholipid complex *in vitro*, intracellular and *ex vivo*. The changes of emission signals of FITC (520 nm) and RB (570 nm) as a function of time during *in vitro* release of (a) physical mixture of RB and FITC labelled phospholipid and (b) FITC labelled RB-PC complex. (c) The fluorescence resonance energy transfer (FRET) efficiency changes and (d) release profile during the *in vitro* release. Fluorescent micrographs showing cellular uptake of RB and FITC labelled phospholipid physical mixture (e) and FITC labelled RB-PC complex (f) over time. Fluorescent micrographs showing cellular release of RB and FITC labelled phospholipid physical mixture (g) and FITC labelled RB-PC complex (h) over time (merge: DAPI+FITC+RB, DAPI (blue)/FITC (green)/RB (red), scale bar represents 100 μm). The changes of quantified fluorescence intensity (i) and FRET efficiency (j) during cellular uptake. The changes of quantified fluorescence intensity (k) and FRET efficiency (l) during cellular release. (m) Images of *ex vivo* RB fluorescent intensity of lung tissues excised at different time post pulmonary administration

Release and lung retention mechanisms of phospholipid complex

To gain a deeper understanding of the sustained release and lung retention effects of phospholipid complexes, we employed a fluorescence resonance energy transfer (FRET) imaging approach to monitor the release kinetics of RB-PC. FRET is a physical phenomenon where excited energy is transferred from one fluorescent group to another. In this process, the excited donor transfers a portion of its energy to the acceptor in a non-radiative manner, leading to the excitation and subsequent fluorescence emission of the acceptor whereas the donor fluorescence is quenched. This energy transfer occurs when the two fluorescent dyes are in close proximity, enabling us to assess the dissociation of fluorophores from the carrier [49].

In this work, RB (exhibiting red fluorescence with excitation/emission wavelengths of 547/570 nm) served as a surrogate of DAS, whereas FITC-labeled phospholipid (displaying green fluorescence with excitation/emission wavelengths of 490/520 nm) was used to characterize the behavior of phospholipids. By capitalizing on FRET, we were able to observe the interaction between RB and FITC within the nanostructure of the complex, thereby elucidating the *in vitro* release kinetics, as well as the cellular uptake and release process of RB-PC. In contrast, measuring the release of DAS-PC in cell culture settings remained challenging due to the intricacies involved in distinguishing between released and encapsulated DAS.

Figure 3a and b demonstrated the temporal variations in the emission signals of FITC (520 nm) and RB (570 nm) during the *in vitro* release of RB-PC and the physical mixture of RB and FITC-labelled phospholipid. The release profiles were indicated by the decrease in RB signal. The fluorescence of FITC gradually increases (Fig. 3b) as RB was released from the nanoparticles, reflecting the weakening and eventual cessation of FRET. On the contrary, the fluorescence intensity of FITC remains constant in the

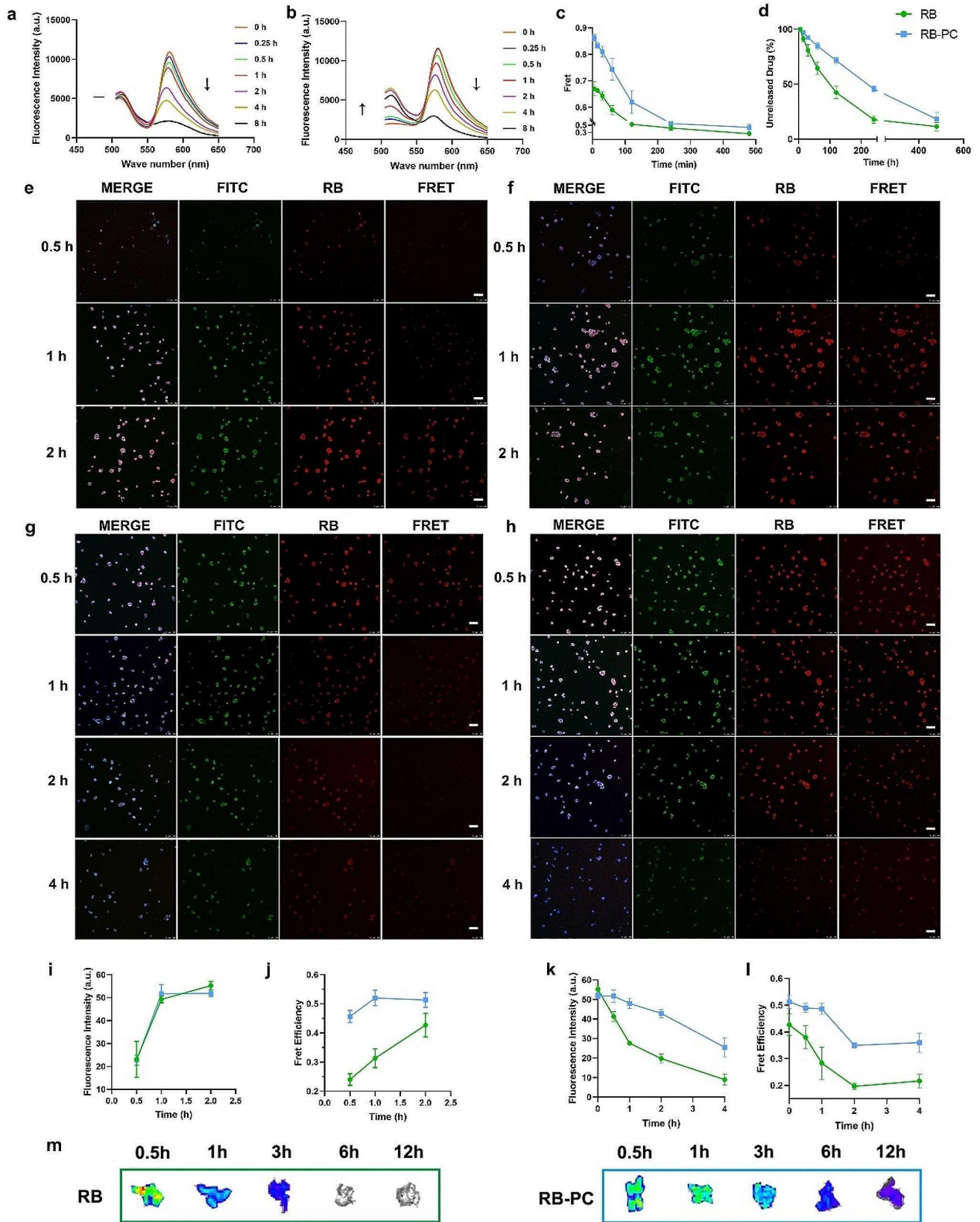
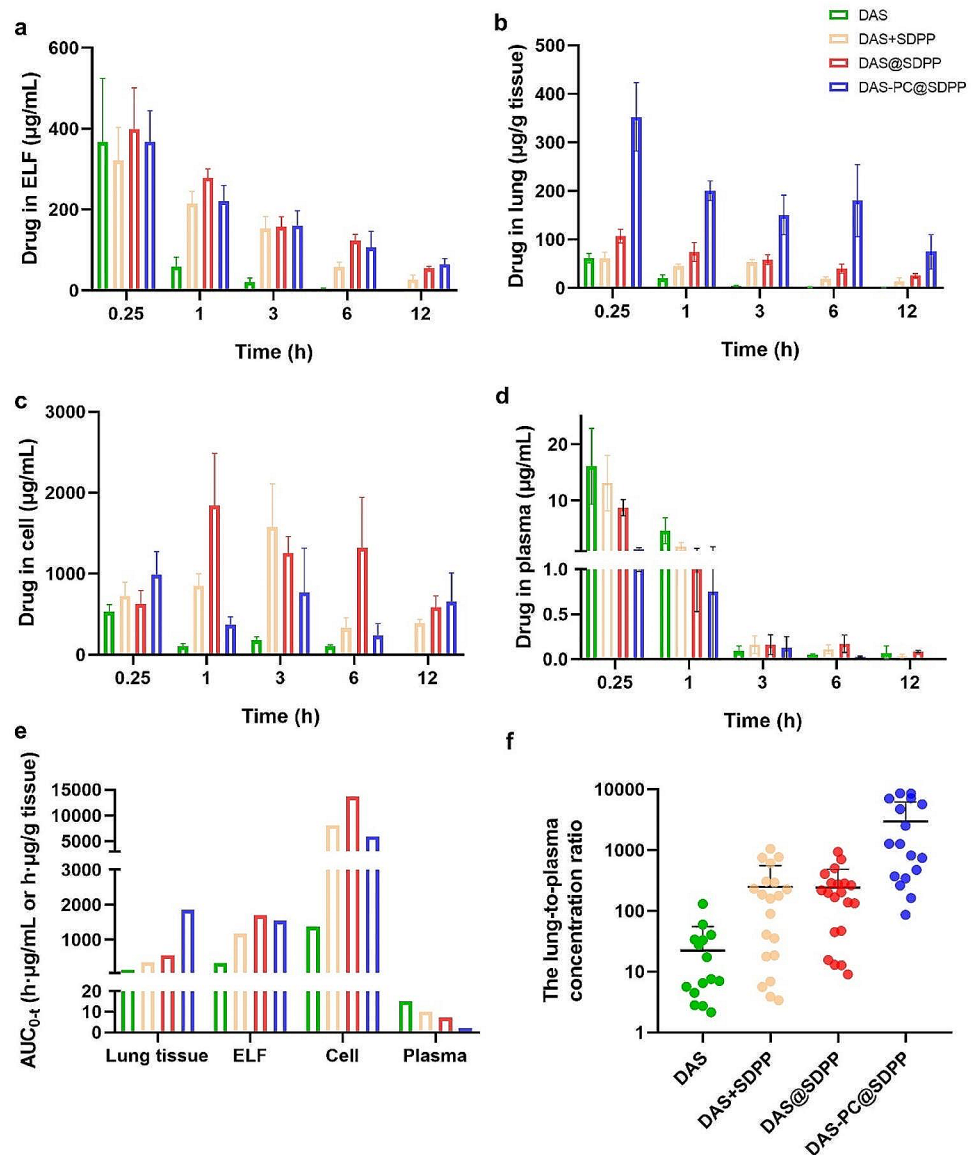


Fig. 4 The concentrations of DAS in (a) lung epithelial lining fluid (ELF), (b) lung tissues after bronchoalveolar lavage, (c) immune cells isolated from the ELF and (d) plasma as a function of time (mean \pm SD, $n=4$), the area under curve (AUC) values (e) and the lung-to-plasma concentration ratios (f) after intratracheal administration of free DAS (green), physical mixture of DAS and SDPP (orange), DAS@SDPP (red) and DAS-PC@SDPP (blue) to mice



physical mixture group (Fig. 3a) as no FRET was observed. This phenomenon was also reflected in the changes of FRET efficiency (Fig. 3c) where the fluorescence ratio changed significantly with the release of RB from the complex. In addition, similar to the *in vitro* release profiles of DAS-PC, the presence of phospholipid delayed the release of RB and the release rates of RB-PC were lower than those of the physical mixture (Fig. 3d).

Subsequently, we conducted cellular uptake and release experiments. Figure 3e and f show that the cellular uptake of RB and FITC increased as a function of time after Calu-3 cells were incubated with the physical mixture of RB and FITC labelled phospholipid or RB-PC, respectively. The amount of RB taken up by cells was quantified by the fluorescence intensity and the results showed that the cellular content of RB increased rapidly and reached a plateau

within 60 min (Fig. 3i). There were no significant differences in the uptake rates between the physical mixture and RB-PC. However, when the FRET ratios were compared, there was a significant difference between the physical mixture and RB-PC. When the cells were incubated with the physical mixture, FRET ratios increased with increasing the incubation time whereas FRET ratios remained almost consistent upon incubation with RB-PC (Fig. 3j). The latter finding suggested that RB was mainly taken up by cells as a form of phospholipid complex.

After cellular uptake of RB, the intracellular release profiles were monitored. Figure 3g and 3h show that the cellular fluorescence intensity of RB and FITC decreased in a time-dependent manner. The cellular fluorescence intensity of RB incubated with the physical mixture decreased more rapidly than that with RB-PC (Fig. 3k) and such findings

were in good agreement with the results that DAS-PC prolonged lung retention (Fig. 2h). The FRET data were indicative of the intracellular disassociation of RB-PC and the result (Fig. 3l) showed that RB-PC exhibited slower disassociation within cells than in the aqueous medium used for in vitro release testing. Based on the above findings, cellular uptake of free water-soluble RB was subjected to rapid release from cells, leading to poor intracellular retention, whereas RB-PC prolonged the intracellular residence time considerably due to slow intracellular disassociation.

To further elucidate whether RB-PC prolonged the retention of RB in the lung in vivo, RB-PC suspension was intratracheally delivered to mice. The results showed that after instillation of free RB physically mixed with phospholipid, the fluorescence in the lung maintained only for 3 h whereas the administration of RB-PC extended the lung retention by 12 h (Fig. 3m).

Pharmacokinetics and lung distribution of DAS formulations

After confirming the sustained release and lung retention effects of DAS-PC and RB-PC, we evaluated the pharmacokinetics and lung distribution of DAS following intratracheal administration of different DAS formulations and the concentrations of DAS in lung epithelial lining fluid (ELF), lung tissues after bronchoalveolar lavage, immune cells isolated from the ELF and plasma as a function of time are shown in Fig. 4 and their pharmacokinetic parameters are listed in SI, Table S2. After intratracheal administration of DAS solution, the drug was rapidly cleared from the ELF with a $T_{1/2}$ of 1.27 h whereas the intratracheal insufflations of DAS powders, i.e. the physical mixture of DAS and SDPP, DAS@SDPP and DAS-PC@SDPP, resulted in decreased absorption clearance from the ELF (Fig. 4a) and increased the $T_{1/2}$ by 3.66–4.78 h. Similar to the in vitro release profiles, the three powder formulations exhibited comparable clearance profiles from the ELF with the mean residence time (MRT) ranging from 3.41 h to 4.23 h. When the relative exposure to ELF was compared, the AUC values of DAS from DAS@SDPP and DAS-PC@SDPP were 5.0-fold and 4.6-fold of free DAS (Fig. 4e and SI, Table S2).

The insufflations of DAS-PC@SDPP achieved always significantly higher lung concentrations of DAS than the intratracheal administration of free DAS, the physical mixture of DAS and SDPP or DAS@SDPP (Fig. 4b). The relative lung exposures of the former were between 3.33-fold and 14.3-fold of the latter three counterparts (Fig. 4e and SI, Table S2). The prolonged lung retention conferred by DAS-PC@SDPP was well consistent with the prolonged intracellular retention conferred by DAS-PC and RB-PC (Figs. 2h and 3k).

The DAS concentrations in immune cells isolated from the ELF were generally higher than the corresponding counterparts in ELF or lung tissues (Fig. 4c). The insufflations of DAS powders resulted in increases in drug exposure to cells by 4.34–9.93 folds compared to instilled DAS solution (Fig. 4e and SI, Table S2).

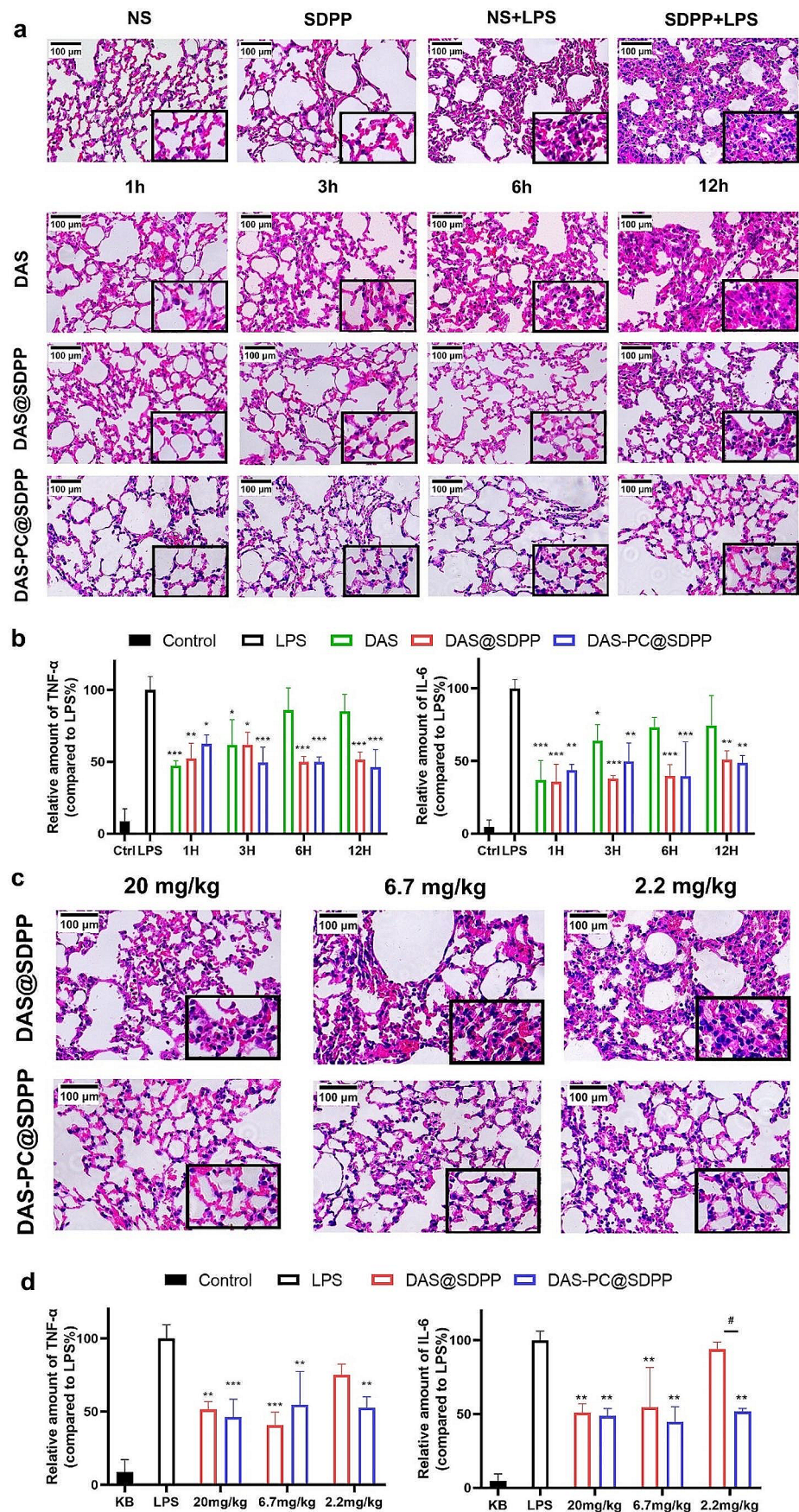
In agreement with previous results [24], instilled DAS solution resulted in rapid absorption into the bloodstream with a T_{max} of 15 min, followed by a rapid decrease in plasma concentration (Fig. 4d). Compared to instillation of DAS solution, insufflations of DAS powders delayed pulmonary absorption of DAS and decreased the plasma bioavailability. The decreased bioavailability might be related to the increased lung affinity conferred by the presence of phospholipid or the formation of DAS-PC. Indeed, as shown in Fig. 4f, the presence of phospholipids increased the lung-to-plasma concentration ratios from 20 to 249 and upon formation of DAS-PC, the ratios further increased to 2952.

Pulmonary anti-inflammatory efficacy in vivo

Next, we test whether the encouraging sustained release and favourable in vivo biodistribution of DAS in immune cells and lung tissues could give a high in vivo anti-inflammatory efficiency. We examined the local anti-inflammatory effect of DAS formulations using LPS-induced acute lung injury mice model. This animal model has been well documented to imitate clinical respiratory diseases, e.g. lung inflammation, bacterial pneumonia and acute respiratory distress syndrome (ARDS), and accumulation of neutrophils in the alveolar or the interstitial space and up-regulation of pro-inflammatory cytokines e.g. interleukin-6 (IL-6) and tumour necrosis factor α (TNF- α), represent typical features of the lung injury and inflammatory responses [50–52]. As shown in Fig. 5a, the intratracheal administration of blank SDPP powders and normal saline (NS) did not cause an inflammatory response in lungs whereas LPS treatment induced a dramatic increase in the number of inflammatory cells (blue spots) in lung tissues and markedly thickened the alveolar walls. The intratracheal administration of DAS formulations decreased the density of inflammatory cells in lung tissues in a time-dependent manner.

All DAS formulations were found to confer anti-inflammatory effects on mouse lungs in terms of the decreased levels of TNF- α and IL-6 in bronchoalveolar lavage fluid (BALF) (Fig. 5b). However, the insufflations of DAS@SDPP and DAS-PC@SDPP prolonged the duration of anti-inflammation as compared to instilled DAS solution. The latter maintained a significant anti-inflammatory effect only for 3 h whereas the former two formulations extended the duration of action to at least 12 h. To understand lung

Fig. 5 Pulmonary anti-inflammatory efficacy of DAS, DAS@SDPP and DAS-PC@SDPP. Representative H&E stained sections of lungs after lipopolysaccharide challenge and treatments with insufflated DAS formulations at a DAS dose of 20 mg/kg (a) or different doses of DAS (c) or different doses of DAS (d). * $P < 0.05$, ** $P < 0.01$, *** $P < 0.001$, as compared to LPS alone; # $P < 0.05$, representing a significant difference between the specified two groups



exposure– anti-inflammatory efficacy relationships within the lungs, mice were pre-treated with insufflations of DAS@SDPP and DAS-PC@SDPP at different doses at 12 h before LPS challenge. As shown in Fig. 5c and d, the two formulations elicited comparable anti-inflammatory effects at doses of 6.6 and 20 mg/kg. However, when the dose was decreased to 2.2 mg/kg, insufflated DAS@SDPP elicited no significant anti-inflammatory effects whereas insufflations of DAS-PC@SDPP maintained the efficacy comparable to the high dose counterparts (e.g., 6.6 mg/kg).

Discussion

In the treatment of respiratory ailments such as pneumonia and ARDS, it is imperative to enhance and prolong the exposure of drugs to respiratory epithelial cells through sustained pulmonary delivery systems. This is necessitated by the fact that systemic delivery efficiency is relatively low due to the unique physiological barrier of the lungs [3, 53]. When considering the potential for clinical application, phospholipid-based particles, such as liposomes and PulmoSphere particles, exhibit superior pulmonary biocompatibility compared to polymer-based particles for sustained pulmonary delivery. However, both liposomes and PulmoSphere particles have their inherent limitations. For instance, inhaled liposomes often demonstrate poor storage stability and challenges in scaling up production, whereas the delayed release of PulmoSphere particles is influenced by the inherent dissolution/release properties of the drug-loaded particles.

In this study, we have developed modified PulmoSphere particles that contained DAS-phospholipid complex to promote the lung retention of drug after pulmonary delivery. The present phospholipid-based delivery system has exhibited several superior features.

Firstly, the system holds significant potential for clinical translation in comparison to polymer-based formulations. This is due to the fact that the present formulation comprises only pulmonary biocompatible excipients, namely phospholipid and CaCl₂. In addition, the total quantity of excipients in the preparation falls well within the maximum daily exposure limit for the inhalation route, as specified in the FDA's Inactive Ingredient Database.

Secondly, the production of the modified PulmoSphere particles can be scaled up more readily using commonly employed techniques like vacuum drying and spray drying, in contrast to liposomes. In addition, the manufacturing process appeared not to affect the physicochemical properties of the incorporated drug-phospholipid complex. Indeed, DAS-phospholipid complex was able to self-assemble into nanoparticles. Upon spray-drying to obtain porous

microparticles with drug phospholipid complex, the rehydrated microparticles discharged drug phospholipid complex without compromising the physicochemical properties.

Thirdly, upon incorporation into a carrier-free dry powder formulation, the modified PulmoSphere particles maintained excellent inhalability of conventional PulmoSphere particles. They exhibited desirable aerodynamic characteristics, ensuring targeted delivery of drug to the peripheral region. The spray-dried porous microparticles containing the DAS-phospholipid complex were shown a high FPF (~60%) and a low MMAD (~2 μm), optimising deposition in the alveolar region.

Fourthly, after deposition in the lung, the phospholipid complex exhibited the ability to prolong drug retention in respiratory epithelial cells *in vitro* and in lung tissues both *in vitro* and *in vivo*. The incorporation of the drug-phospholipid complex into the PulmoSphere particles through spray-drying did not compromise the nanostructure of the phospholipid complex. This ensured not only enhanced lung retention but also intracellular retention in respiratory epithelial cells and immune cells.

Compared to free drug or spray-dried porous particles containing free drug, the spray-dried particles loaded with the phospholipid complex demonstrated a prolonged duration of anti-inflammatory action in the lung, even at reduced doses. Previous studies have consistently shown that the lung-targeted anti-inflammatory effect is primarily linked to lung exposure of drugs, rather than plasma bioavailability [54]. Similarly, in this study, the pulmonary anti-inflammatory efficacy was closely associated with lung exposure, rather than plasma bioavailability. LPS-induced lung injury leads to the infiltration of activated inflammatory cells into the interstitial space and ELF [52, 55]. Targeted delivery of drugs to these immune cells in the lungs has been proven to enhance anti-inflammatory responses [56, 57]. Nonetheless, airway epithelial dysfunction was regarded to play a vital role in the development of acute lung injury and ARDS, making airway epithelial cells a crucial therapeutic target for novel treatment strategies [58]. In this work, the local anti-inflammatory effects of inhaled DAS powders were associated with drug exposure to lung tissues, rather than immune cells. Specifically, DAS-PC@SDPP provided a 3.33-fold increase in drug exposure to lung tissues compared to DAS@SDPP. Consequently, insufflations of DAS-PC@SDPP at a dose of 2.2 mg/kg elicited comparable anti-inflammatory effects to those of DAS@SDPP at a dose of 6.6 mg/kg, despite the latter providing higher drug exposure to immune cells. These findings confirm that increasing and prolonging drug exposure in respiratory epithelial cells contributes significantly to relieving lung inflammation induced by LPS.

Understanding the exposure-response relationship between pharmacokinetics and pharmacodynamics has key implications for the development of novel inhalation products. In the literature, inhaled liposomes and phospholipid-based particles prolonged lung retention generally due to sustained drug release and decreased cellular uptake and hence, the availability of released drug to epithelial cells was limited, leading to a poor exposure-response relationship [12, 21, 22, 39, 59, 60]. In contrast, the present phospholipid complex based formulation prolonged lung retention by sustained intracellular release, and therefore it could increase and prolong drug exposure to epithelial cells, conferring elevated local therapeutic efficacy.

Conclusion

The present study has reported a novel phospholipid-based delivery system, achieved by integrating the DAS-phospholipid complex into spray-dried PulmoSphere particles, enabling sustained pulmonary delivery. Compared to conventional PulmoSphere particles, the DAS-phospholipid complex loaded counterpart conferred not only excellent aerodynamic properties but also an extended intracellular retention in respiratory epithelial cells and immune cells. The improved drug exposure to the airway epithelial cells but not necessarily to the immune cells in the ELF was responsible for the prolonged duration of pulmonary anti-inflammation, even at decreased doses. Overall, the DAS-phospholipid complex loaded microparticles with pulmonary biocompatibility, inhalability and extended intracellular retention offers a possibility for treating respiratory diseases, e.g. pneumonia and ARDS.

Supplementary Information The online version contains supplementary material available at <https://doi.org/10.1007/s13346-024-01626-6>.

Author contributions Chen WY: Investigation, Writing- Original draft & Formal analysis; Wei JX: Formal analysis, Validation; Yu CY: Investigation; Liu CY: Resources; Liao YH: Conceptualization, Writing-Review & Editing, Funding acquisition. All authors read and approved the final manuscript.

Funding This work was supported by the National Natural Science Foundation of China (Grant No. 82173983) and the CAMS Innovation Fund for Medical Sciences (CIFMS, Grant No. 2021-I2M-1-048).

Data availability All data generated or analyzed during this study are included in this published article.

Declarations

Ethics approval Animal procurement and experiments were subjected to approval by the Animal Ethics Committee of the Institute of Medicinal Plant Development, Chinese Academy of Medical Sciences

& Peking Union Medical College, ethical approval number SLXD-20211025012.

Consent to participate This study does not involve human subjects.

Consent for publication This study does not contain any individual person's data in any form.

Competing interests The authors declare no conflict of interest.

References

- Ruaro B, Salton F, Braga L, Wade B, Confalonieri P, Volpe MC, Baratella E, Maiocchi S, Confalonieri M. The history and mystery of alveolar epithelial type II cells: focus on their physiologic and pathologic role in lung. *Int J Mol Sci.* 2021;22(5):2566. <https://doi.org/10.3390/ijms22052566>.
- Mizgerd JP. Acute lower respiratory tract infection. *N Engl J Med.* 2008;358(7):716–27. <https://doi.org/10.1056/NEJMr074111>.
- Raviv AS, Alyan M, Egorov E, Zano A, Harush MY, Pieters C, Korach-Rechtman H, Saadya A, Kaneti G, Nudelman I, Farkash S, Flikshain OD, Mekies LN, Koren L, Gal Y, Dor E, Shainsky J, Shklover J, Adir Y, Schroeder A. Lung targeted liposomes for treating ARDS. *J Control Release.* 2022;346:421–33. <https://doi.org/10.1016/j.jconrel.2022.03.028>.
- Patton JS, Fishburn CS, Weers JG. The lungs as a portal of entry for systemic drug delivery. *Proc Am Thorac Soc.* 2004;1(4):338–44. <https://doi.org/10.1513/pats.200409-049TA>.
- Loira-Pastoriza C, Todoroff J, Vanbever R. Delivery strategies for sustained drug release in the lungs. *Adv Drug Deliv Rev.* 2014;75:81–91. <https://doi.org/10.1016/j.addr.2014.05.017>.
- Honeybourne D, Baldwin DR. The site concentrations of antimicrobial agents in the lung. *J Antimicrob Chemother.* 1992;30(3):249–60. <https://doi.org/10.1093/jac/30.3.249>.
- Strong P, Ito K, Murray J, Rapeport G. Current approaches to the discovery of novel inhaled medicines. *Drug Discov Today.* 2018;23(10):1705–17. <https://doi.org/10.1016/j.drudis.2018.05.017>.
- Wang Y, Chen L. Lung tissue distribution of drugs as a key factor for COVID-19 treatment. *Br J Pharmacol.* 2020;177(21):4995–6. <https://doi.org/10.1111/bph.15102>.
- Calfee CS, Janz DR, Bernard GR, May AK, Kangelaris KN, Matthay MA, Ware LB. Distinct molecular phenotypes of direct vs indirect ARDS in single-center and multicenter studies. *Chest.* 2015;147(6):1539–48. <https://doi.org/10.1378/chest.14-2454>.
- Liang Z, Ni R, Zhou J, Mao S. Recent advances in controlled pulmonary drug delivery. *Drug Discov Today.* 2015;20(3):380–9. <https://doi.org/10.1016/j.drudis.2014.09.020>.
- Hu X, Yang FF, Liao YH. Pharmacokinetic considerations of inhaled pharmaceuticals for systemic delivery. *Curr Pharm Des.* 2016;22(17):2532–48. <https://doi.org/10.2174/1381612822666160128150005>.
- Gupta V, Gupta N, Shaik IH, Mehvar R, McMurtry IF, Oka M, Nozik-Grayck E, Komatsu M, Ahsan F. Liposomal fasudil, a rho-kinase inhibitor, for prolonged pulmonary preferential vasodilation in pulmonary arterial hypertension. *J Control Release.* 2013;167(2):189–99. <https://doi.org/10.1016/j.jconrel.2013.01.011>.
- Anderson CF, Chakraborty RW, Su H, Mitrut RE, Cui H. Interface-enrichment-induced instability and drug-loading-enhanced stability in inhalable delivery of supramolecular filaments. *ACS Nano.* 2019;13(11):12957–68. <https://doi.org/10.1021/acsnano.9b05556>.

14. Garbuzenko OB, Kuzmov A, Taratula O, Pine SR, Minko T. Strategy to enhance lung cancer treatment by five essential elements: inhalation delivery, nanotechnology, tumor-receptor targeting, chemo- and gene therapy. *Theranostics*. 2019;9(26):8362–76. <https://doi.org/10.7150/thno.39816>.
15. Kirtane AR, Verma M, Karandikar P, Furin J, Langer R, Traverso G. Nanotechnology approaches for global infectious diseases. *Nat Nanotechnol*. 2021;16(4):369–84. <https://doi.org/10.1038/s41565-021-00866-8>.
16. La Zara D, Sun F, Zhang F, Franek F, Balogh Sivars K, Horn-dahl J, Bates S, Brännström M, Ewing P, Quayle MJ, Petersson G, Folestad S, van Ommen JR. Controlled pulmonary delivery of carrier-free budesonide dry powder by atomic layer deposition. *ACS Nano*. 2021;15(4):6684–98. <https://doi.org/10.1021/acsnano.0c10040>.
17. Ma SQ, Cong ZQ, Wei JX, Chen WY, Ge D, Yang FF, Liao YH. Pulmonary delivery of size-transformable nanoparticles improves tumor accumulation and penetration for chemo-sonodynamic combination therapy. *J Control Release*. 2022;350:132–45. <https://doi.org/10.1016/j.jconrel.2022.08.003>.
18. Jones RM, Neef N. Interpretation and prediction of inhaled drug particle accumulation in the lung and its associated toxicity. *Xenobiotica*. 2012;42(1):86–93. <https://doi.org/10.3109/00498254.2011.632827>.
19. Healy AM, Amaro MI, Paluch KJ, Tajber L. Dry powders for oral inhalation free of lactose carrier particles. *Adv Drug Deliv Rev*. 2014;75:32–52. <https://doi.org/10.1016/j.addr.2014.04.005>.
20. Ong W, Nowak P, Cu Y, Schopf L, Bourassa J, Enlow E, Moskowitz SM, Chen H. Sustained pulmonary delivery of a water-soluble antibiotic without encapsulating carriers. *Pharm Res*. 2016;33(3):563–72. <https://doi.org/10.1007/s11095-015-1808-x>.
21. Meers P, Neville M, Malinin V, Scotto AW, Sardaryan G, Kurumunda R, Mackinson C, James G, Fisher S, Perkins WR. Biofilm penetration, triggered release and in vivo activity of inhaled liposomal amikacin in chronic pseudomonas aeruginosa lung infections. *J Antimicrob Chemother*. 2008;61(4):859–68. <https://doi.org/10.1093/jac/dkn059>.
22. Okusanya OO, Bhavnani SM, Hammel J, Minic P, Dupont LJ, Forrest A, Mulder GJ, Mackinson C, Ambrose PG, Gupta R. Pharmacokinetic and pharmacodynamic evaluation of liposomal amikacin for inhalation in cystic fibrosis patients with chronic pseudomonas infection. *Antimicrob Agents Chemother*. 2009;53(9):3847–54. <https://doi.org/10.1128/AAC.00872-08>.
23. Cipolla D, Shekunov B, Blanchard J, Hickey A. Lipid-based carriers for pulmonary products: preclinical development and case studies in humans. *Adv Drug Deliv Rev*. 2014;75:53–80. <https://doi.org/10.1016/j.addr.2014.05.001>.
24. Chen WY, Wang YS, Liu CY, Ji YB, Yang FF, Liao YH. Comparison of pulmonary availability and anti-inflammatory effect of dehydroandrographolide succinate via intratracheal and intravenous administration. *Eur J Pharm Sci*. 2020;147:105290. <https://doi.org/10.1016/j.ejps.2020.105290>.
25. Weers J, Tarara T. The PulmoSphere™ platform for pulmonary drug delivery. *Ther Deliv*. 2014;5(3):277–95. <https://doi.org/10.4155/tde.14.3>.
26. Hirst PH, Pitcairn GR, Weers JG, Tarara TE, Clark AR, Dellamary LA, Hall G, Shorr J, Newman SP. In vivo lung deposition of hollow porous particles from a pressurized metered dose inhaler. *Pharm Res*. 2002;19(3):258–64. <https://doi.org/10.1023/a:1014482615914>.
27. Geller DE, Weers J, Heuerding S. Development of an inhaled dry-powder formulation of tobramycin using PulmoSphere™ technology. *J Aerosol Med Pulm Drug Deliv*. 2011;24(4):175–82. <https://doi.org/10.1089/jamp.2010.0855>.
28. Israel S, Kumar A, DeAngelis K, Aurivillius M, Dorinsky P, Roche N, Usmani OS. Pulmonary deposition of budesonide/glycopyrronium/formoterol fumarate dihydrate metered dose inhaler formulated using co-suspension delivery technology in healthy male subjects. *Eur J Pharm Sci*. 2020;153:105472. <https://doi.org/10.1016/j.ejps.2020.105472>.
29. Bombardelli E, Curri SB, Loggia Rd, Negro PD, Gariboldi P, Tubaro A. Complexes between phospholipids and vegetal derivatives of biological interest. *Fitoterapia*. 1989;60:1–9.
30. Khan J, Alexander A, Ajazuddin, Saraf S, Saraf S. Recent advances and future prospects of phyto-phospholipid complexation technique for improving pharmacokinetic profile of plant actives. *J Control Release*. 2013;168(1):50–60. <https://doi.org/10.1016/j.jconrel.2013.02.025>.
31. Barani M, Sangiovanni E, Angarano M, Rajizadeh MA, Mehrbani M, Piazza S, Gangadharappa HV, Pardakhty A, Mehrbani M, Dell'Agli M, Nematollahi MH. Phytosomes as innovative delivery systems for phytochemicals: a comprehensive review of literature. *Int J Nanomed*. 2021;16:6983–7022. <https://doi.org/10.2147/IJN.S318416>.
32. Cook RO, Pannu RK, Kellaway IW. Novel sustained release microspheres for pulmonary drug delivery. *J Control Release*. 2015;104(1):79–90. <https://doi.org/10.1016/j.jconrel.2005.01.003>.
33. Wei JX, Li CY, Chen WY, Cong YJ, Liu CY, Yang FF, Liao YH. The pulmonary biopharmaceutics and anti-inflammatory effects after intratracheal and intravenous administration of re-du-ning injection. *Biomed Pharmacother*. 2023;160:114335. <https://doi.org/10.1016/j.biopha.2023.114335>.
34. Chen H, Kim S, He W, Wang H, Low PS, Park K, Cheng JX. Fast release of lipophilic agents from circulating PEG-PDLLA micelles revealed by in vivo forster resonance energy transfer imaging. *Langmuir*. 2008;24(10):5213–7. <https://doi.org/10.1021/la703570m>.
35. Chaurasiya B, Zhou M, Tu J, Sun C. Design and validation of a simple device for insufflation of dry powders in a mice model. *Eur J Pharm Sci*. 2018;123:495–501. <https://doi.org/10.1016/j.ejps.2018.08.010>.
36. Qiu Y, Liao Q, Chow MYT, Lam JKW. Intratracheal administration of dry powder formulation in mice. *J Vis Exp*. 2020;161:e61469. <https://doi.org/10.3791/61469>.
37. Rayamajhi M, Redente EF, Condon TV, Gonzalez-Juarrero M, Riches DW, Lenz LL. Non-surgical intratracheal instillation of mice with analysis of lungs and lung draining lymph nodes by flow cytometry. *J Vis Exp*. 2011;51:e2702. <https://doi.org/10.3791/2702>.
38. Furuie H, Saisho Y, Yoshikawa T, Shimada J. Intrapulmonary pharmacokinetics of s-013420, a novel bicyclic antibacterial, in healthy Japanese subjects. *Antimicrob Agents Chemother*. 2010;54(2):866–70. <https://doi.org/10.1128/AAC.00567-09>.
39. Fu TT, Cong ZQ, Zhao Y, Chen WY, Liu CY, Zheng Y, Yang FF, Liao YH. Fluticasone propionate nanosuspensions for sustained nebulization delivery: an in vitro and in vivo evaluation. *Int J Pharm*. 2019;572:118839. <https://doi.org/10.1016/j.ijpharm.2019.118839>.
40. Angelico R, Ceglie A, Sacco P, Colafemmina G, Ripoli M, Mangia A. Phyto-liposomes as nanoshuttles for water-insoluble silybin-phospholipid complex. *Int J Pharm*. 2014;471(1–2). <https://doi.org/10.1016/j.ijpharm.2014.05.026>. 173–81.
41. Oomens J, Steill JD. Free carboxylate stretching modes. *J Phys Chem A*. 2008;112(15):3281–3. <https://doi.org/10.1021/jp801806e>.
42. Lv Y, Guo Y, Luo X, Li H. Infrared spectroscopic study on chemical and phase equilibrium in triethylammonium acetate. *Sci China Chem*. 2012;55:1688–94. <https://doi.org/10.1007/s11426-012-4634-6>.
43. Nie H, Mo H, Zhang M, Song Y, Fang K, Taylor LS, Li T, Byrn SR. Investigating the interaction pattern and structural

- elements of a drug-polymer complex at the molecular level. *Mol Pharm*. 2015;12(7):2459–68. <https://doi.org/10.1021/acs.molpharmaceut.5b00162>.
44. Chi C, Zhang C, Liu Y, Nie H, Zhou J, Ding Y. Phytosome-nanosuspensions for silybin-phospholipid complex with increased bioavailability and hepatoprotection efficacy. *Eur J Pharm Sci*. 2020;144:105212. <https://doi.org/10.1016/j.ejps.2020.105212>.
 45. Pomeranke A, Lea SR, Herrick S, Lindsay MA, Singh D. Characterization of tlr-induced inflammatory responses in copd and control lung tissue explants. *Int J Chron Obstruct Pulmon Dis*. 2016;11:2409–17. <https://doi.org/10.2147/COPD.S105156>.
 46. Ayyar VS, Song D, DuBois DC, Almon RR, Jusko WJ. Modeling corticosteroid pharmacokinetics and pharmacodynamics, part I: determination and prediction of dexamethasone and methylprednisolone tissue binding in the rat. *J Pharmacol Exp Ther*. 2019;370(2):318–26. <https://doi.org/10.1124/jpet.119.257519>.
 47. Van Holsbeke C, De Backer J, Vos W, Marshall J. Use of functional respiratory imaging to characterize the effect of inhalation profile and particle size on lung deposition of inhaled corticosteroid/long-acting β 2-agonists delivered via a pressurized metered-dose inhaler. *Ther Adv Respir Dis*. 2018;12:1753466618760948. <https://doi.org/10.1177/1753466618760948>.
 48. Jain H, Bairagi A, Srivastava S, Singh SB, Mehra NK. Recent advances in the development of microparticles for pulmonary administration. *Drug Discov Today*. 2020;25(10):1865–72. <https://doi.org/10.1016/j.drudis.2020.07.018>.
 49. Chen T, He B, Tao J, He Y, Deng H, Wang X, Zheng Y. Application of forster resonance energy transfer (fret) technique to elucidate intracellular and in vivo biofate of nanomedicines. *Adv Drug Deliv Rev*. 2019;143:177–205. <https://doi.org/10.1016/j.addr.2019.04.009>.
 50. Knapp S. LPS and bacterial lung inflammation models. *Drug Discovery Today: Disease Models*. 2009;6(4):113–8. <https://doi.org/10.1016/j.ddmod.2009.08.003>.
 51. Chen H, Bai C, Wang X. The value of the lipopolysaccharide-induced acute lung injury model in respiratory medicine. *Expert Rev Respir Med*. 2010;4(6):773–83. <https://doi.org/10.1586/ers.10.71>.
 52. Aeffner F, Bolon B, Davis IC. Mouse models of acute respiratory distress syndrome: a review of analytical approaches, pathologic features, and common measurements. *Toxicol Pathol*. 2015;43(8):1074–92. <https://doi.org/10.1177/0192623315598399>.
 53. Qiao Q, Liu X, Yang T, Cui K, Kong L, Yang C, Zhang Z. Nanomedicine for acute respiratory distress syndrome: the latest application, targeting strategy, and rational design. *Acta Pharm Sin B*. 2021;11(10):3060–91. <https://doi.org/10.1016/j.apsb.2021.04.023>.
 54. Ho DK, Nichols BLB, Edgar KJ, Murgia X, Loretz B, Lehr CM. Challenges and strategies in drug delivery systems for treatment of pulmonary infections. *Eur J Pharm Biopharm*. 2019;144:110–24. <https://doi.org/10.1016/j.ejpb.2019.09.002>.
 55. Moldoveanu B, Otmishi P, Jani P, Walker J, Sarmiento X, Guardiola J, Saad M, Yu J. Inflammatory mechanisms in the lung. *J Inflamm Res*. 2009;2:1–11.
 56. Wang Z, Li J, Cho J, Malik AB. Prevention of vascular inflammation by nanoparticle targeting of adherent neutrophils. *Nat Nanotechnol*. 2014;9(3):204–10. <https://doi.org/10.1038/nnano.2014.17>.
 57. Liu C, Liu YH, Xi L, He Y, Liang YM, Mak J, Mao SR, Wang ZP, Zheng Y. Interactions of inhaled liposome with macrophages and neutrophils determine particle biofate and anti-inflammatory effect in acute lung inflammation. *ACS Appl Mater Interfaces*. 2023;15(1):479–93. <https://doi.org/10.1021/acsami.2c17660>.
 58. Wang XD, Adler KB, Erjefalt J, Bai CX. Airway epithelial dysfunction in the development of acute lung injury and acute respiratory distress syndrome. *Expert Rev Respir Med*. 2007;1(1):149–55. <https://doi.org/10.1586/17476348.1.1.149>.
 59. Weers J. Comparison of phospholipid-based particles for sustained release of ciprofloxacin following pulmonary administration to bronchiectasis patients. *Pulm Ther*. 2019;5(2):127–50. <https://doi.org/10.1007/s41030-019-00104-6>.
 60. He Y, Liu C, Han R, Liang YM, Mak JCW, Zhu YH, Li HF, Zheng Y. Reducing systemic absorption and macrophages clearance of genistein by lipid-coated nanocrystals for pulmonary delivery. *Chin Chem Lett*. 2023;34(1):107484. <https://doi.org/10.1016/j.ccllet.2022.04.082>.

Publisher's Note Springer Nature remains neutral with regard to jurisdictional claims in published maps and institutional affiliations.

Springer Nature or its licensor (e.g. a society or other partner) holds exclusive rights to this article under a publishing agreement with the author(s) or other rightsholder(s); author self-archiving of the accepted manuscript version of this article is solely governed by the terms of such publishing agreement and applicable law.